Molecular Au(I) Complexes in the Photosensitized Photocatalytic CO_2 Reduction Reaction

Shakeyia Davis,[a] *Dinesh Nugegoda,*[a] *Joshua Tropp,*[b] *Jason D. Azoulay,*[b] *and Jared H. Delcamp*[a]

[a] Department of Chemistry and Biochemistry, University of Mississippi, University, MS 38677, USA

[b] School of Polymer Science and Engineering, University of Southern Mississippi, Hattiesburg, MS 39406, USA

corresponding author email: delcamp@olemiss.edu

Abstract: Five Au-complexes are evaluated for the reduction reaction of CO_2 via cyclic voltammetry and in a photocatalytic system. Electrochemically, the complexes were all evaluated for pre-association with CO_2 prior to electrochemical reduction, and for thermodynamic favorability for CO_2 reduction in photocatalytic systems. The complexes were evaluated in photocatalytic reactions using an Ir-based photosensitizer and a sacrificial electron donor for the conversion of CO_2 to CO. Au-complex counter ions effects on the photocatalytic reaction were analyzed by varying weakly coordinating counter ions with significant performance changes noted. At low Au-complex concentrations, a high TON value of 700 was observed.

Introduction:

The solar driven conversion of CO_2 to a fuel is an attractive process to meet growing energy demands. Gold-based heterogeneous and multinuclear homogeneous Au-catalysts are well known in the literature to drive this process.[1-5] While these complex systems are interesting, studying mononuclear homogeneous systems can be informative, readily tunable, and simpler to understand. As such, we sought to probe the behavior of four mononuclear gold complexes and one dinuclear gold complex in the catalytic photosensitized CO_2 reduction reaction driven by sunlight (Figure 1).

The five Au complexes selected for catalysis studies are readily available commercially (Figure 1). Triphenylphosphine complexes **1** and **2** differ in the anionic ligand as either a bis(trifluoromethanesulfonyl)imide (TFSI) or a chloride allowing for the comparison of a weakly coordinating TFSI counter ion with a more strongly coordinating chloride ion. Complexes **2**, **3**, and **5** differ in the neutral ligand (L) on the L-Au-Cl complexes studied, which allows for the comparison of triphenylphosphine (TPP, complex **2**), tri-*o*-tolylphosphine (TTP, complex **5**), and 1,3-bis(2,6-di-isopropylphenyl)imidazol-2-ylidene as a *N*-heterocyclic carbene (NHC, complex **3**). Finally, a comparison of the mononuclear complex **2** is possible with dinuclear complex **4** which has two diphenylphosphine ligated Au atoms linked by a methylene bridge. Herein, the Au complex reduction potentials are determined through cyclic voltammetry analysis under argon and CO_2 to ensure favorable energetics for the photocatalytic system using an iridium photosensitizer ($Ir(ppy)_3$, where ppy is 2-phenylpyridine). The complexes are also evaluated within a photocatalytic reaction with a sacrificial electron donor (SED), 1,3-dimethyl-2-phenyl-2,3-dihydro-1*H*-benzo[*d*]-imidazole (BIH).[6]

Materials and Methods:

Cyclic voltammetry (CV) analysis was done with a CH instruments electrochemical analyzer (CHI600E). Cyclic voltammograms were generated with a Ag-wire as the reference electrode, platinum as the counter electrode, and glassy carbon as the working electrode in a 0.1 M tetrabutylammonium hexafluorophosphate (NBu_4PF_6, purchased from Beantown Chemicals, 98.0% purity, used as received) solution as the supporting electrolyte. All electrochemical measurements were taken in anhydrous acetonitrile (MeCN, purchased from Fisher, 99.5% purity, distilled over CaH_2) at a scan rate of 100 mV/s. For each experiment the catalyst concentration was kept constant at 1 mM (**1** was purchased from Aldrich at 99.9% purity and used without further purification; **2** was purchased from Strem at 99.9% purity and used without further purification; **3** was purchased from Aldrich at 97.0% purity and used without further purification; **4** was purchased from Aldrich at 97.0% purity and used without further purification; **5** was purchased from Aldrich at 95.0% purity and used without further purification). Before each measurement, the solution was degassed with argon or CO_2 (for ~5 min). To avoid concentration changes, the solvent height in the sealed 3-neck electrochemical cell was marked after reaction setup before degassing.[7] The mixture was then diluted with pure MeCN (~2 mL) and degassed with argon (purchased from NexAir, 99.999% purity) or CO_2 (purchased from NexAir, 99.99% purity) until the solvent level returned to the marked volume. During cyclic voltammetry scans, the sweep width window was set to approximately the electrolyte/solvent window reduction limit.

Each photocatalytic reaction was set up in a 17 mL Pyrex tube[8] by adding BIH (0.005 g, 0.02 mmol),[6] MeCN (6 ml), $Ir(ppy)_3$ (purchased from Ark Pharm, 98.0% purity, used as received, 0.2 ml from a 1×10^{-3} M in MeCN solution), and catalyst (0.2 ml from a 1×10^{-3} M in MeCN solution). Studies were also conducted with *N,N*-dimethylformamide (DMF, purchased from

Fisher at 99.9% purity, and was freshly distilled prior to use with a 20% volume forecut discarded and 20% volume left in the distillation flask) in place of MeCN and $Ru(bpy)_3^{2+}$ ($Ru(bpy)_3Cl_2$ was purchased from Tokyo Chemical Industry at 98.0% purity, and was used without further purification) in place of $Ir(ppy)_3$. Each tube was sealed with a rubber septum and parafilm. Solutions were bubbled vigorously with CO_2 for at least 15 minutes until the solution volume reached 1.9 ml and then 0.1 ml of N_2 degassed triethylamine (TEA, purchased from Fisher, 99.0% purity, used as received) was injected into to the mixture. A 150 W Xe-lamp based small collimated beam solar simulator equipped with an AM 1.5 filter (Sciencetech SF-150C) was used as the irradiation source. Headspace analysis was performed using a VICI gas tight syringe with a stopcock and a custom Agilent 7890B Gas Chromatography (GC) instrument equipped with Agilent Porapak Q 6ft, 1/8 in. O.D. column. Quantitation of CO and CH_4 were made using an FID detector, while H_2 was quantified using a TCD detector. All GC response calibrations were done using standards purchased from BuyCalGas.com. Before GC injection, headspace samples were taken and the pressure was adjusted to atmospheric pressure by pressurizing the sample (300 μL taken from the headspace then compressed to 250 μL) then submerging the tip of the sealed gas tight syringe into diethyl ether.[8] The syringe was opened and gas was observed exiting the needle tip. The syringe was then sealed, removed from the diethyl ether solution and injected into the GC mentioned above. To analyze for formate production upon reaction completion, 0.8 mL of the reaction solution was taken into a syringe and added to a 4 mL vial along with 36 μL of DBU (1,8-diazabicyclo(5.4.0)undec-7-ene, purchased from Aldrich, 98.0% purity, used as received).[9] The mixture was sonicated for 10 minutes at room temperature and 1.16 mL of a *d*3-MeCN (purchased from Cambridge Isotope Laboratories, 99.5% purity, used as received) *p*-xylene solution (1.19 mM concentration of *p*-xylene, purchased from Aldrich, 99.0% purity, used as received) was added to the mixture. The vial was thoroughly mixed, then a ^{1}H NMR spectrum was taken on a 500 MHz NMR or 300 MHz NMR with an extended D1-delay of 10 seconds and a minimum of 200 scans (example Figure S1). The ratio of the formate peak (~8.7 ppm) and the xylene peak (~7.0 ppm) were then compared to a calibration curve generated through the analysis of known concentrations of formate (0.0 mM, 0.1 mM, 1.0 mM, and 10.0 mM solutions). Through this method, the concentration of formate could be evaluated accurately through a trendline having an R^2 value of 0.997 and 0.999. All NMR spectra were evaluated with MestReNova software to ensure a level baseline in the analyte region prior to integrating peaks.

Silver metathesis reaction general procedure: An Au-complex (0.05 mmol) and an Ag-salt (0.05 mmol: AgTFSI was purchased from Alfa Aesar at 97.0% purity and used as received; $AgBF_4$ was purchased from Aldrich at 98.0% purity and used as received; AgOTf was purchased from Aldrich at >99% purity and used as received; $AgSbF_6$ was purchased from Beantown Chemicals at 99.0% purity and used as received) was added to a vial followed by the addition of dichloromethane (DCM, purchased from Fisher at 99.9% purity and passed through a solvent purification system using aluminum oxide) (10 mL). After adding the solvent, the solution was rapidly stirred for 30 minutes at room temperature. Once stirring was stopped, the reaction mixture was syringe filtered first through a 0.45 μm Nylon syringe filter, and then filtered through a thin pad of Celite under N_2. After filtration, the solvent was removed the complex was used directly in a photocatalytic reaction.

Results and Discussion:

The cyclic voltammogram of complex **1** under argon shows a reduction wave with a peak at –3.0 V versus ferrocenium/ferrocene (Figure 2, Table S1). For all of the Au complexes analyzed, all reduction waves were found to be irreversible. Upon exchange of the atmosphere with CO_2, a dramatic shift in curve shape is observed with a shift of about 300 mV toward less negative potentials. A change in thermodynamics toward more positive reduction potentials in the presence of CO_2 is indicative of a pre-coordination event of CO_2 to the metal center before reduction occurs. Additionally, the current increases under CO_2 which indicates a catalytic process is taking place since the concentration of catalyst is held constant at 1 mM. The reduction of complex **2** under argon shows minimal changes relative to **1** in terms of thermodynamic shifts; however, changing the anionic ligand from TFSI to Cl^- again reveals a significant pre-coordination event of CO_2 prior to reduction of the complex with a larger shift of about 600 mV toward more positive potentials. From the peak current response under CO_2 (i_{cat}) and under argon (i_p) at a respective reduction wave, an estimation of the relative rates of the various catalysts can be obtained by analyzing the ratio of i_{cat}/i_p from CV experiments.[10] **1** shows a substantially larger current increase upon the addition of CO_2 with an i_{cat}/i_p ratio of 32 compared to 1.2 for **2**. These results show the anionic ligand has a dramatic impact on catalyst rates and a lesser influence on thermodynamics when TFSI and Cl^- are compared.

Complex **3** shows a reduction peak at –2.99 V under argon which is similar to that of complex **2** despite dramatically different neutral ligands (NHC versus TPP). For complex **3**, again a shift toward more positive reduction potentials is observed by about 300 mV; however, no significant change in current response is observed at the first or second reduction waves which present as shoulders in the CV spectrum under CO_2 and argon, respectively. This indicates complex **3** is not behaving catalytically under these conditions, but does bind CO_2 which could be beneficial for CO_2 electrochemical sensing applications.[11] It is not apparent why the NHC ligand halts catalysis from these studies, but presumably a carbon-bound Au-complex intermediate has been significantly stabilized.

Complex **4** has a significantly more positive first reduction potential at –1.8 V with no current increase or potential shift upon changing the atmosphere to CO_2 from argon. A second reduction wave at –2.7 V is observed under argon. When CO_2 is used as the atmosphere, the second reduction wave shifts to –2.2 V with a unique series of about 3 features at higher current than the catalyst reduction wave under argon appearing at –2.7 V. This indicates complex **4** is catalytically competent for the reduction of CO_2 with a pre-catalysis association of CO_2 likely occurring after the first reduction of the complex. The complexity of the cyclic voltammogram is likely correlated to complex **4** having two possible reactive centers which may participate in cooperative catalysis to access catalytic intermediates not accessible to the mononuclear complexes studied here.

Complex **5** shows a more positive reduction potential than comparable complex **2** under argon (–2.33 V versus –3.04 V, respectively). The anionic ligand is held constant as Cl^-, so the observed change in reduction potentials must arise from the differences of TPP and TTP which have measurably different Tolman electronic parameters (2069 cm^{-1} versus 2067 cm^{-1}) and substantially different cone angles (145° versus 194°). Under CO_2, the reduction wave shift toward more positive potentials is modest at about 100 mV at the wave onsets. This may indicate a weak per-coordination of CO_2 to complex **5** before reduction.[11] The reduced binding strength of CO_2 relative to **2** is likely due to the increased sterics of the TTP ligand shielding the metal center. However, despite the increased sterics, complex **5** shows a significantly higher i_{cat}/i_p ratio than complex **2** (7.1 s^{-1} versus 1.2 s^{-1}) which indicates a more reactive active complex is formed. Among the halide complexes studied, complex **5** shows the fastest catalytic rates for CO_2 reduction which may be due in part to the strong donation strength of the TTP ligand. Overall the following order for rates of catalysis is observed **1** >> **5** > **4** > **2** >> **3** (not catalytic).

Interestingly, complexes **1**, **2**, and **5** show catalytic activity at the first reduction wave. Given that CO is forming (see discussion below) as a 2-electron reduction product from CO_2, catalytic reactivity at the first reduction wave is unusual. Within the literature, this is most commonly observed with NHC complexes which are very strong σ-donating ligands.[6, 12-16] In this study, it is unclear if this reduction behavior is a result of the use of phosphine ligands behaving similar to NHC complexes or if the Au metal center is uniquely behaving.

Notably, all of the complexes studied have significantly negatively catalytic reduction potentials ranging from –2.40 V to –2.73 V. At these potentials, a strongly reducing photosensitizer (PS) such as $Ir(ppy)_3$ is needed with a reported reduction potential of –2.61 V in MeCN to adequately deliver electrons to the Au complexes.[9] $Ir(ppy)_3$ has a positive excited-state reduction potential at 0.06 V, and a strong SED such as BIH (which is oxidized at –0.10 V) is desirable for reasonable quenching constants.[9] Since BIH generates an acidic proton upon being oxidized, TEA is added to the reaction mixture to react with BIH radical cation to ensure irreversible electron transfers take place.[17] Under these conditions, **1** generated 5 turnover numbers (TONs) of CO as confirmed by GC analysis with a maximum turnover frequency (TOF) for a 1 hour period of 3.2 h^{-1} (Figures 3 and S1, Table 1). Catalysts **2**, **4**, and **5** show very similar TON and TOF values of 2 and 0.8-0.9, respectively. The slower rate of catalysis for these complexes is consistent with the estimated TOF parameter trend from the CV studies. Complex **3** shows no catalytic production of CO which is consistent with the CV studies above as well. No significant quantities of CH_4 (GC), methanol (^1H NMR), or formate (^1H NMR) were observed in these reactions (see Figure S1 for an example GC spectrum and see Figure S2 for an example NMR spectrum).

In addition to the rate of the reaction, the quantum yield for each catalyst was measured at 1 hour (Table S2).[18, 19] The order of quantum yields is as follows: **1** >> **5** = **2** ≅ **4** >> **3** ranging from 0.103% to 0.001%. The quantum yields are indicative of homogeneous bimolecular electron transfer catalysis at <1% for all of the catalysts.[19] Additionally, the initial rates for the first data points shows no change with time from an induction period, which indicates homogeneous catalysis whereas heterogenous catalyzed reactions often have slow initial induction periods.[20] The reproducibility of these reactions at each data point is high at < ± 5% error with all reactions being the average of at least 2 experiments. A high level or reproducibility (especially at early timepoints) is most commonly attributed to homogenous catalysis systems as well.[20]

To probe the importance of each component in the reaction (Table 1, entries 7-13; Figure 3), reagents were removed or removed and replaced with alternative reagents systematically. Removing CO_2 led to 0 turnovers of CO in this system which indicates the CO produced is derived from CO_2. BIH is necessary to observe a turnover, which is expected since an easily oxidizable SED is needed to donate electrons to a photoexcited $Ir(ppy)_3$. Removal of the Au complexes shows no TONs of CO which indicates that Au is necessary for catalysis. $Ir(ppy)_3$ was also found to be required for catalysis which indicates the Au catalysts are behaving as electrocatalysts within this photocatalytic system rather than as direct photocatalysts. Replacing $Ir(ppy)_3$ with the weaker reducing $Ru(bpy)_3^{2+}$ (–2.61 V versus –1.72 V, respectively) gave no appreciable CO production which is consistent with the energetics of the Au complexes requiring a strongly reducing photosensitizer. Removing TEA from the photocatalytic system reduces the TON value from 5 to 3. This is likely because TEA aids in limiting back electron transfer events from reduced $Ir(ppy)_3$ to oxidized BIH by driving a chemical deprotonation reaction.[17] Finally, solvent was found to not be a critical component to reactivity since replacing MeCN with *N*,*N*-dimethylformamide (DMF) led to a similar TON value (5 versus 7, respectively).

Complexes **1** and **2** differ in the coordination strength of the ionic ligand, which results in a significant change in catalytic reactivity. Exchanging the anionic ligand for other weakly coordinating or "non-coordinating" anions available in the literature could further enhance reactivity. Silver salt metathesis with complex **2** provides a convenient method to introduce a range of anionic groups (Figure 3). To ensure an efficiently working metathesis protocol without harming catalysis, we first sought to develop a procedure for the conversion of **2** to **1** with AgTFSI without loss of photocatalytic reactivity in the system (Table 1, entries 14-16; Figure 3). Initial attempts to run the metathesis reaction on **2** in MeCN either without filtering the Ag^+ salts or filtering via nylon syringe filter led to lower reactivity at 1 TON and 3 TON, respectively, relative to complex **1**. This suggests that the Ag^+ ions poison the photocatalytic reaction, and care must be taken to thoroughly remove the silver salts through filtration, and the use of a solvent with low solubility for the silver salts is attractive. Changing the solvent to DCM for the salt metathesis reaction followed by filtration of the salts with both a syringe filter and through a pad of Celite followed by evaporation of the solvent, led to an identical TOF value for **1** and **2** after the metathesis protocol. This suggests the toluene adduct has minimal influence on catalytic activity since a very similar catalytic performance was realized with **2** after salt metathesis in DCM in the absence of toluene.

With a protocol for halide exchange to alternate anionic counter ions in hand, several weakly coordinating counter ions were investigated including BF_4, OTf, and SbF_6 which were introduced via a salt metathesis of **2** (Table 1, entries 17-19; Figure 3). Interestingly, a significant dependence on the "non-coordinating" counter ion was observed with the following order obtained: BF_4 > TFSI > OTf >> SbF_6 (ranging from 7 to 0 TON). This suggests a significant interaction between the Au atom and each of these anions. Given the strong dependence of reactivity on the counter ion, complexes **3** and **4** were analyzed with AgTFSI as the metathesis reagent (Table 1, entries 20 and 21; Figure 3). Complex **3** with a chloride ion was found to be non-reactive; however, stoichiometric reactivity (1 TON of CO) was observed for **3** after AgTFSI metathesis. Similarly, the reactivity of **4** increased to 3 TON from 2 TON for complex **4** after metathesis which gives a total of 1.5 TON per Au atom with the TFSI counter ion.

Finally, it is well-described in the literature that many photocatalytic reactions proceed to significantly higher TON values upon lowering the concentration of a catalyst.[8, 18, 21, 22] The concentration of catalyst **1** was probed at a lower concentration of 1 μM relative to the standard concentration used in these studies at 0.1 mM. Reducing the catalyst concentration raised the maximum TON value observed by 2 orders of magnitude to give a value of 700 TON (Table 1, entry 6; Figure 3). This increased value was accompanied by a substantial increase in TOF value as well at 34 h^{-1} versus 3.2 h^{-1} at high concentration. The origin of this increase in TON based on concentration is not obvious from these studies, but suggests either limiting catalyst-catalyst interactions or increasing the effective concentration of reducing reagents per catalyst results in a more durable catalyst system.

Conclusions:

Five Au(I) complexes were analyzed in a photocatalytic system for the reduction of CO_2. The four phosphine ligated complexes were found to electrocatalytically react CO_2 with the weakly coordinating TFSI ligand having the fastest reaction rates. All complexes were found to pre-associate with CO_2 prior to reduction by shifts in the reduction potentials under CO_2 relative to argon. In the presence of Ir(ppy)$_3$, the four phosphine ligated complexes were found to reduce CO_2 to CO selectively during photocatalysis. Initial catalytic rates and data reproducibility, suggest these complexes are acting as homogeneous catalysts. Lowering the catalyst concentration was found to substantially increase the number of turnovers observed at up to 700 TON. This system provides a rare example of mononuclear Au complexes active for CO_2 reduction, which could be beneficial for better understanding the ubiquitous Au heterogeneous catalysts reported in the literature.

Supplementary Material:

Additional electrochemical data, an example GC trace, an example ^{1}H NMR analysis, and additional TON versus time plots are all available as part of the electronic supplementary materials.

Acknowledgements:

The authors gratefully acknowledge NSF award OIA-1632825 for funding this research. J. T. acknowledges traineeship support from the NSF NRT program “Interface” (DGE 1449999) through the University of Southern Mississippi.

References:

1 V. R. Jupally, A. C. Dharmaratne, D. Crasto, A. J. Huckaba, C. Kumara, P. R. Nimmala, N. Kothalawala, J. H. Delcamp and A. Dass: $Au_{137}(SR)_{56}$ nanomolecules: composition, optical spectroscopy, electrochemistry and electrocatalytic reduction of CO_2. *Chem. Commun.*, **50**, 9895 (2014).

2 D. R. Kauffman, D. Alfonso, C. Matranga, H. Qian and R. Jin: Experimental and computational investigation of Au_{25} clusters and CO_2: a unique interaction and enhanced electrocatalytic activity. *J. Am. Chem. Soc.*, **134**, 10237 (2012).

3 Y. Chen, C. W. Li and M. W. Kanan: Aqueous CO2 reduction at very low overpotential on oxide-derived Au nanoparticles. *J. Am. Chem. Soc.*, **134**, 19969 (2012).

4 K. Sun, T. Cheng, L. Wu, Y. Hu, J. Zhou, A. Maclennan, Z. Jiang, Y. Gao, W. A. Goddard, 3rd and Z. Wang: Ultrahigh Mass Activity for Carbon Dioxide Reduction Enabled by Gold-Iron Core-Shell Nanoparticles. *J. Am. Chem. Soc.*, **139**, 15608 (2017).

5 H. Kim, H. S. Park, Y. J. Hwang and B. K. Min: Surface-Morphology-Dependent Electrolyte Effects on Gold-Catalyzed Electrochemical CO_2 Reduction. *J. Phys. Chem. C*, **121**, 22637 (2017).

6 A. J. Huckaba, E. A. Sharpe and J. H. Delcamp: Photocatalytic Reduction of CO_2 with Re-Pyridyl-NHCs. *Inorg. Chem.*, **55**, 682 (2016).

7 J. D. Cope, N. P. Liyanage, P. J. Kelley, J. A. Denny, E. J. Valente, C. E. Webster, J. H. Delcamp and T. K. Hollis: Electrocatalytic reduction of CO_2 with CCC-NHC pincer nickel complexes. *Chem. Commun.*, **53**, 9442 (2017).

8 S. Das, R. R. Rodrigues, R. W. Lamb, F. Qu, E. Reinheimer, C. M. Boudreaux, C. E. Webster, J. H. Delcamp and E. T. Papish: Highly Active Ruthenium CNC Pincer Photocatalysts for Visible-Light-Driven Carbon Dioxide Reduction. *Inorg. Chem.*, **58**, 8012 (2019).

9 R. R. Rodrigues, C. M. Boudreaux, E. T. Papish and J. H. Delcamp: Photocatalytic Reduction of CO_2 to CO and Formate: Do Reaction Conditions or Ruthenium Catalysts Control Product Selectivity? *ACS Appl. Energy Mater.*, **2**, 37 (2019).

10 N. P. Liyanage, H. A. Dulaney, A. J. Huckaba, J. W. Jurss and J. H. Delcamp: Electrocatalytic Reduction of CO_2 to CO With Re-Pyridyl-NHCs: Proton Source Influence on Rates and Product Selectivities. *Inorg. Chem.*, **55**, 6085 (2016).

11 M. H. Schmidt, G. M. Miskelly and N. S. Lewis: Effects of Redox Potential, Steric Configuration, Solvent, and Alkali Metal Cations on the Binding of Carbon Dioxide to Cobalt(I) and Nickel(I) Macrocycles. *J. Am. Chem. Soc.*, **112**, 3420 (1990).

12 J. Agarwal, T. W. Shaw, C. J. Stanton, 3rd, G. F. Majetich, A. B. Bocarsly and H. F. Schaefer, 3rd: NHC-containing manganese(I) electrocatalysts for the two-electron reduction of CO_2. *Angew. Chem. Int. Ed.*, **53**, 5152 (2014).

13 T. Jin, D. He, W. Li, C. J. Stanton, S. A. Pantovich, G. F. Majetich, H. F. Schaefer, J. Agarwal, D. Wang and G. Li: CO_2 reduction with Re(I)-NHC compounds: driving selective catalysis with a silicon nanowire photoelectrode. *Chem. Commun.*, **52**, 14258 (2016).

14 C. J. Stanton, 3rd, C. W. Machan, J. E. Vandezande, T. Jin, G. F. Majetich, H. F. Schaefer, 3rd, C. P. Kubiak, G. Li and J. Agarwal: Re(I) NHC Complexes for Electrocatalytic Conversion of CO_2. *Inorg. Chem.*, **55**, 3136 (2016).

15 C. J. Stanton, 3rd, J. E. Vandezande, G. F. Majetich, H. F. Schaefer, 3rd and J. Agarwal: Mn-NHC Electrocatalysts: Increasing π Acidity Lowers the Reduction Potential and Increases the Turnover Frequency for CO_2 Reduction. *Inorg. Chem.*, **55**, 9509 (2016).

16 C. A. Carpenter, P. Brogdon, L. E. McNamara, G. S. Tschumper, N. I. Hammer and J. H. Delcamp: A Robust Pyridyl-NHC-Ligated Rhenium Photocatalyst for CO_2 Reduction in the Presence of Water and Oxygen. *Inorganics*, **6**, 22 (2018).

17 Y. Kuramochi, O. Ishitani and H. Ishida: Reaction mechanisms of catalytic photochemical CO_2 reduction using Re(I) and Ru(II) complexes. *Coord. Chem. Rev.*, **373**, 333 (2018).

18 N. P. Liyanage, W. Yang, S. Guertin, S. Sinha Roy, C. A. Carpenter, R. E. Adams, R. H. Schmehl, J. H. Delcamp and J. W. Jurss: Photochemical CO_2 reduction with mononuclear and dinuclear rhenium catalysts bearing a pendant anthracene chromophore. *Chem. Commun.*, **55**, 993 (2019).

19 J. Bonin, M. Robert and M. Routier: Selective and efficient photocatalytic CO_2 reduction to CO using visible light and an iron-based homogeneous catalyst. *J. Am. Chem. Soc.*, **136**, 16768 (2014).

20 J. A. Widegren and R. G. Finke: A review of the problem of distinguishing true homogeneous catalysis from soluble or other metal-particle heterogeneous catalysis under reducing conditions. *J. Mol. Cat. A: Chem.*, **198**, 317 (2003).

21 H. Shirley, X. Su, H. Sanjanwala, K. Talukdar, J. W. Jurss and J. H. Delcamp: Durable Solar-Powered Systems with Ni-Catalysts for Conversion of CO_2 or CO to CH_4. *J. Am. Chem. Soc.*, **141**, 6617 (2019).

22 V. S. Thoi, N. Kornienko, C. G. Margarit, P. Yang and C. J. Chang: Visible-light photoredox catalysis: selective reduction of carbon dioxide to carbon monoxide by a nickel N-heterocyclic carbene-isoquinoline complex. *J. Am. Chem. Soc.*, **135**, 14413 (2013).

Figure Captions:

Figure 1. Structures of Au(I) complexes studied in photosensitized CO_2 reduction reactions with an iridium photosensitizer and a sacrificial electron donor.

Figure 2. Cyclic voltammetry of **1-5** under argon and CO_2. The electrolyte is 0.1 M Bu_4NPF_6 in MeCN with a glassy carbon working electrode, Ag wire reference, and Pt counter electrode. Note: The Y-axis scales vary between graphs so that catalyst reduction waves can be observed for the less active catalysts.

Figure 3. A: TON versus time plot for CO production with complexes **1-5**. B: Turnover number versus time plot examining the removal or the removal and replacement of various components of the photocatalytic system. C: Turnover number versus time plot for various salt metathesis route generated catalysts. D: Turnover number versus time plot for complex **1** at 1 μM concentration. E: Silver salt metathesis scheme for the conversion of **2** to **1** as an example of how the complexes were prepared for graph C.

Table 1. Photocatalytic CO$_2$ reduction reaction data using complexes **1-5**.

Entry	**Complex**	**Change**	**TON$_{max}$**	**TOF$_{max}$ (h^{-1})**
			CO [H$_2$]	CO
Standard Conditions with Commercial Catalysts				
1	1	None	5 [0]	3.2
2	2	None	2 [0]	0.8
3	3	None	trace [0]	0.1
4	4	None	2 [0]	0.8
5	5	None	2 [0]	0.9
6	1	1 μM cat. concentration	700 [0]	34
Controls				
7	1	No CO$_2$	0 [0]	0.0
8	1	DMF as solvent	7 [0]	2.8
9	1	No BIH	0 [0]	0.0
10	1	Ru(bpy)$_3^{2+}$ as PS	trace [0]	0.4
11	1	No TEA	3 [0]	1.2
12	1	No Au	0 [0]	0.0
13	1	No Ir(ppy)$_3$	0 [0]	0.0
Standard Conditions with In Situ *Prepared Catalysts*				
14	2	AgTFSI, MeCN, no filter	1 [0]	0.2
15	2	AgTFSI, MeCN, syringe filter	3 [0]	1.9
16	2	AgTFSI, DCM, syringe filter	5 [0]	4.2
17	2	AgBF$_4$, DCM, syringe filter	7 [0]	4.5
18	2	AgOTf, DCM, syringe filter	3 [0]	2.0
19	2	AgSbF$_6$, DCM, syringe filter	0 [0]	0.4
20	3	AgTFSI, DCM, syringe filter	1 [0]	0.3
21	4	AgTFSI, DCM, syringe filter	3 [0]	2.2

TOC Image:

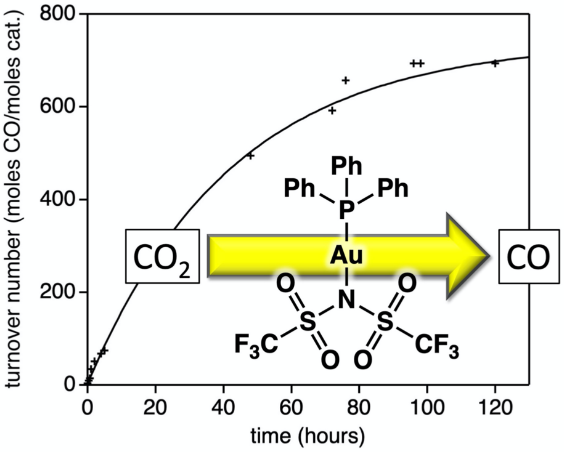

turnover number (moles CO/moles cat.)
800
600
400
200
0
0
20
40
60
80
100
120
time (hours)
CO2
CO
Ph
Ph
Ph
P
Au
N
O
O
O
O
S
S
F3C
CF3